# Sensitive Detection of a Gaseous Analyte with Low-Power Metal–Organic Framework Functionalized Carbon Nanotube Transistors

*Sandeep Kumar,\* Simone Dehm, Laura Wieland, Abhinav Chandresh, Lars Heinke, Benjamin S. Flavel, and Ralph Krupke\**

**A highly sensitive and low-power sensing platform for detecting ethanol molecules by interfacing high-purity, large-diameter semiconducting carbon nanotube transistors with a metal–organic framework layer is presented. The new devices outperform similar graphene-based metal–organic framework devices by several orders of magnitude in terms of sensitivity and power consumption, and can detect extremely low ethanol concentrations down to sub-ppb levels while consuming only picowatts of power. The exceptional sensor performance results from the nanotube transistor's high on/off ratio and its sensitivity to charges, allowing for ultra-low power consumption. The platform can also compensate for shifts in threshold voltage induced by ambient conditions, making it suitable for use in humid air. This novel concept of MOF/CNTFETs could be customized for detecting various gaseous analytes, leading to a range of ultra-sensitive and ultra-low power sensors.**

## 1. Introduction

Gas sensing based on 1D and 2D nanomaterials has been recognized as a promising route to enhance sensor performance in terms of sensitivity, response time, power consumption, and fabrication costs.[1] However, these sensors often not only respond to the specific gas molecule targeted, but also to other molecules that may be present in the surrounding environment or indeed moisture. One way to overcome this problem is to combine a material that provides an intentional selectivity, with a device that provides sufficient read-out sensitivity. Recently, we introduced such a platform for sensing molecules by growing a metal–organic framework (MOF) onto a graphene field-effect transistor (GFET).[2] This combination of a charge-sensitive GFET[3] in combination with a MOF that can selectively host molecules[4] led to a $Cu_2(BDC)_2$-MOF/GFET sensor that is capable of selectively detecting ethanol.[2] The read-out mechanism of the sensor is based on the interaction of the alcohol with the MOF/GFET interface, which causes a build-up of charge close to the GFET. These charges induce a shift in the Dirac voltage and lead to a change in the conductance of the GFET. Since graphene has no bandgap, GFETs have no off-state, and the charge-induced conductance modulation is accordingly limited. To enhance the sensitivity of MOF/FET sensors, the graphene in the readout transistor needs to be substituted with a surface-charge sensitive material that has a band gap. Semiconducting single-walled carbon nanotubes (s-SWCNTs) are ideal candidates since s-SWCNTs are known to yield transistors with very large on/off ratios when fabricated from high-purity material.[5,6] At the same time, a carbon nanotube field-effect transistor (CNTFET) is highly susceptible to environmental charges, whereby the shift in the CNT-FET switching voltage due to charging depends on the nanotube bandgap and diameter.[7] Therefore, in this work we have used large-diameter, high-purity s-SWCNTs and manufactured the MOF/CNTFET devices with a process flow adapted from the previous MOF/GFET study. The resulting CNT-based devices show a four-order of magnitude improved sensitivity to ethanol compared to graphene-based devices. The devices also have very low power consumption, operate in ambient air, have a response time on the scale of seconds, and can be rapidly reset by current-annealing. In the past, a large amount of work has been done in combining carbon nanotubes with metal–organic frameworks to form hybrid structures and composite materials,[8] and

S. Kumar, S. Dehm, L. Wieland, B. S. Flavel, R. Krupke
Institute of Nanotechnology
Karlsruhe Institute of Technology
76021 Karlsruhe, Germany
E-mail: sandeep.kumar@kit.edu; ralph.krupke@kit.edu

L. Wieland, R. Krupke
Department of Materials Science
Technical University of Darmstadt
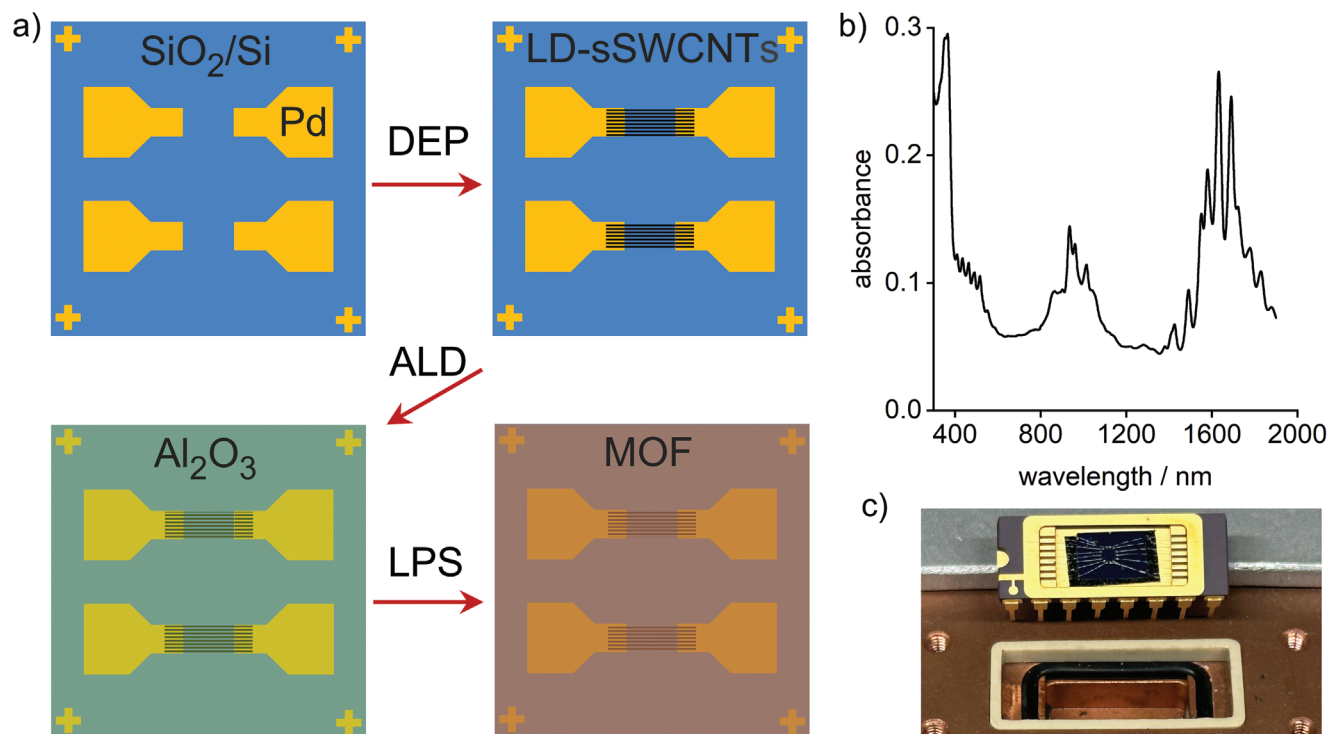64287 Darmstadt, Germany

A. Chandresh, L. Heinke
Institute of Functional Interfaces
Karlsruhe Institute of Technology
76021 Karlsruhe, Germany

R. Krupke
Institute of Quantum Materials and Technologies
Karlsruhe Institute of Technology
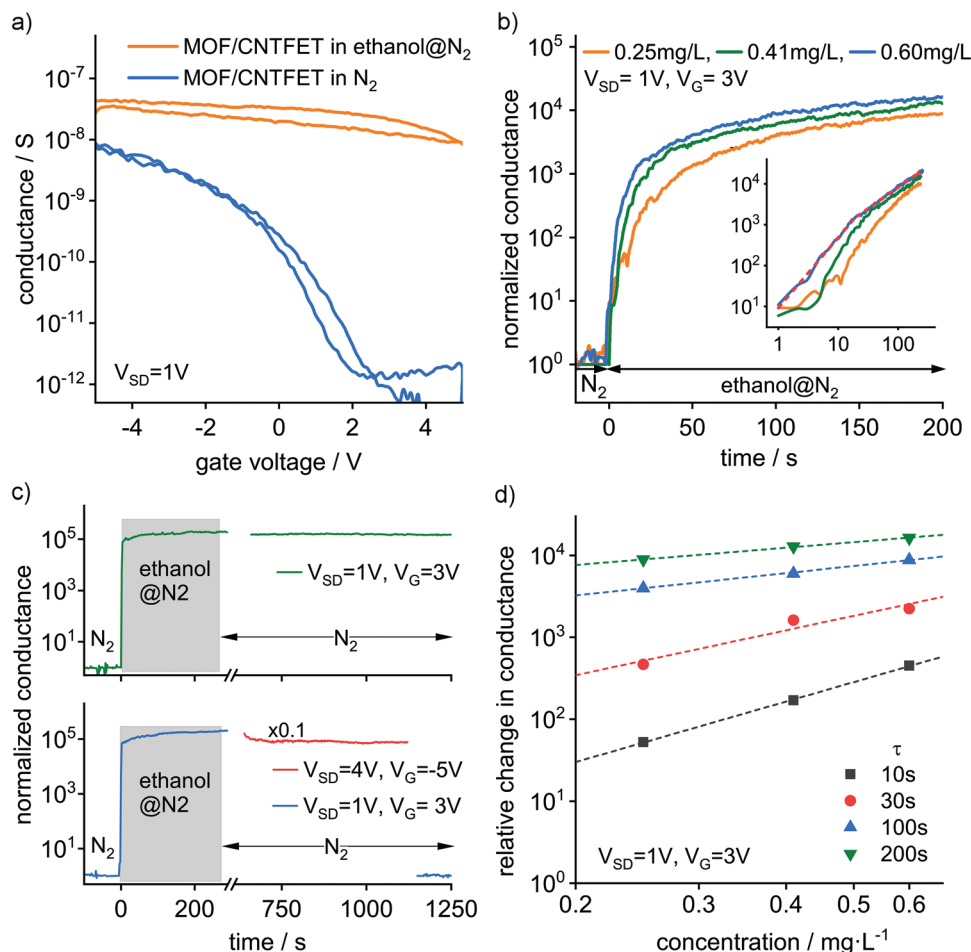76021 Karlsruhe, Germany

**Figure 1.** Fabrication of MOF/CNTFET devices. a) Process flow: large-diameter semiconducting single-walled carbon nanotubes (LD-sSWCNTs) deposited by dielectrophoresis (DEP) on Pd electrodes and $SiO_2$/p-Si substrate, forming a CNTFET with the Si as back-gate. $Al_2O_3$ grown by atomic layer deposition (ALD), and $Cu_2(BDC)_2$-MOF by liquid phase synthesis (LPS). b) Absorbance of the LD-sSWCNT dispersion (1 cm quartz cuvette). c) Wire-bonded and packaged sensor next to the sensing cavity, onto which the package gets mounted head-over. Overview with piping is shown in Figure S9, Supporting Information.

conducting MOFs have been used as a channel material in devices.[9–12] However, MOFs are often insulating or have semiconducting properties that are not suitable for FET operation, and therefore those cases where MOFs can be used as a channel material are rather limited. The substantial innovation of this work is to provide a universal platform that is based on a high-performance carbon nanotube FET onto which any type of MOF can be grown. There have been a few recent reports where MOFs have been grown on nanowire FETs, organic FETs, $MoS_2$-FET,[13–15] and on graphene-FETs.[2] But up to now, no work has been reported where MOFs have been grown on CNTFETs. The major advantage of using a CNTFET as a read-out transistor is that it combines a high on/off ratio at low power consumption with an extremely high sensitivity to charges in its vicinity. This leads in combination with a metal–organic framework to exceptional sensor performance and constitutes a novel route and a major advancement to ultra-sensitive, low-power sensing devices which are required in a world that is increasingly reliant on sensors.

## 2. Results and Discussion

The MOF/CNTFET sensors were fabricated by the process flow shown in **Figure 1**a, with details given in materials and methods. Briefly, Pd/Cr source-drain electrodes with 1 µm gap size were defined by electron-beam lithography and sputtering on 300 nm $SiO_2$/p-Si. In toluene suspended and purified s-SWCNTs with a

diameter of 1.6±0.4 nm were then site-selectively deposited between the electrodes by dc-dielectrophoresis.[16] The absorption spectrum of the s-SWCNT suspension is shown in Figure 1b. On top of the devices, 5 nm $Al_2O_3$ was grown by atomic layer deposition (ALD) by subsequent pulses of trimethylaluminum (TMA) and ozone/water to provide the surface hydroxyl groups that are required for the MOF growth and to electrically isolate the SWCNTs and the electrodes from the MOF. Finally, a $Cu_2(BDC)_2$-MOF with 100 nm nominal thickness was grown by liquid-phase synthesis[17,18] using a spray synthesis, following our previous MOF/GFET work,[2] where we have shown that the ALD-grown $Al_2O_3$ layer remains intact after the MOF synthesis and that a continuous and smooth interface forms between the MOF and the $Al_2O_3$ layer. After fabrication, the devices (Figure 1c) were wired to a ceramic package, mounted to a gas-sensing cavity of volume ≈1 cm$^3$, and connected to a gas line system.[2,19] A four-way valve enables instantaneous switching between gases, and the conditions were controlled by pressure gauges and flow meters (dosing valves). Devices were exposed to air and $N_2$, and to alcohol molecules in the air and in $N_2$ by purging air or $N_2$ through ethanol ($C_2H_5OH$). The relative humidity and alcohol concentrations were monitored with commercial sensors. The MOF/CNTFETs were activated by purging with $N_2$, a process that serves to desorb residual solvent molecules from the MOF pores.[2,20] The gate-voltage dependencies of the device conductance were measured with a semiconductor parameter analyzer at 300 K, using the doped silicon as the back-gate. Optical

**ADVANCED
SCIENCE NEWS**

www.advancedsciencenews.com

**ADVANCED
ELECTRONIC
MATERIALS**

www.advelectronicmat.de

**Figure 2.** MOF/CNTFET response and sensitivity. a) transconductance measured in $N_2$ and in ethanol in $N_2$, b) response of device conductance to different ethanol concentrations with double-logarithmic scaling at inset, c) device reset procedure as described in the main text, d) relative change in conductance $\Delta G/G$ for different ethanol concentrations measured for different waiting times $\tau$, dashed lines are fits (see Table 1).

microscopy images of the devices (Figure S1, Supporting Information), scanning electron microscopy (SEM) images from the devices (Figure S2, Supporting Information), X-ray diffraction (XRD) analysis of the MOF layer (Figure S3, Supporting Information), energy-dispersive X-ray (EDX) analysis (Figure S4, Supporting Information), Raman spectroscopy data (Figure S5, Supporting Information), scanning electron micrograph of pristine CNTFET (Figure S6, Supporting Information), transconductance data of pristine CNTFET (Figure S7, Supporting Information), effect of reset on the transconductance data (Figure S8, Supporting Information), and photography and schematic drawing of the gas sensing setup (Figure S9, Supporting Information) are provided in the supporting information.

**Figure 2**a shows the transconductance curve of a MOF/CNTFET device and its response to ethanol molecules. At first, it is noticeable that the hysteresis and the doping are small, which is unusual for CNT devices in contact with oxide dielectrics such as $SiO_2$ and $Al_2O_3$. Due to ambient processing steps, these oxides are terminated with hydroxyl groups and covered with water molecules, which normally give rise to a hole doping of the SWCNT and hysteresis via electron trapping.[21–23] Figure S7, Supporting Information shows such a pristine CNTFET device,

which due to its large hole doping is not suitable for ethanol sensing. However, due to the MOF synthesis, the OH groups are consumed by the chemical reaction with the copper acetate that anchors the MOF to the alumina. Also, solvent molecules are removed by the activation process, which in total leads to weakly doped SWCNTs and a low-hysteresis in the devices.[2] Upon exposure to ethanol molecules, the devices become severely hole-doped, and the threshold voltage shifts beyond the studied gate-voltage range. In the previous MOF/GFET study, the Dirac voltage shifted from 0 to +20 V. With the MOF/CNTFET devices, we have refrained from sweeping to such large gate voltages, which would be required to determine the shift in threshold voltage and hence the doping. Instead, we have not exceeded the presented gate-voltage range to avoid trapping of charges in the vicinity of the nanotube, which for CNTFETs starts at lower gate-voltages compared to graphene devices because of nanotube-curvature induced field-enhancement. Nevertheless, in order to operate the sensor it is not necessary to know the precise doping level, but rather it requires an appropriate selection of the gate-voltage $V_G$, such that the change in conductance upon ethanol exposure is maximized. This is the case for the MOF/CNTFET device at $V_G = +3$ V. At this gate voltage, the

**ADVANCED
SCIENCE NEWS**

www.advancedsciencenews.com

**ADVANCED
ELECTRONIC
MATERIALS**

www.advelectronicmat.de

device switches from the off-state into the on-state when exposed to ethanol molecules, and the conductance changes by four orders of magnitude. Thanks to the large on/off ratio of the CNTFET, this is three to four orders of magnitude more responsive than our previous MOF/GFETs sensors operated under similar conditions.[2] Figure 2b shows the time dependence of the device conductance upon exposure to different ethanol concentrations. The devices react rapidly as the conductance increases by orders of magnitude within a few seconds. The inset shows that the device has two characteristic time scales and that it reacts faster in the first 10 s. A fast initial response is expected from the shape of the transconductance curves in Figure 2a. When switching from $N_2$ to ethanol@$N_2$, the concentration of ethanol molecules increases, and the blue curve shifts with time to increasingly larger positive gate voltages (yellow curve). Thereby, a rapid initial increase in the conductance is induced by the large sub-threshold slope of the transconductance curve. The data in Figure 2a,b shows that the threshold gate-voltage changes from +4 to $\approx$0 V within the first 10 s upon switching from $N_2$ to ethanol@$N_2$. When switching back from ethanol@$N_2$ to $N_2$, the reverse shift in the threshold occurs much slower and if we keep the biasing conditions set to those which are optimum for sensing (green trace in Figure 2c) it takes hours for the conductance to reach the initial value. However, we can quickly reset the sensor by applying an intermediate biasing condition that leads to rapid current-induced heating of the sensor.[2] CNTs are an ideal material to make low-power FETs that have low energy loss and low heat dissipation, however, also CNTFETs dissipate energy when increasing the source-drain bias. The source–drain current times the bias is the power that is dissipated by the CNTs, which heats the nearby $Al_2O_3$/MOF interface and causes the thermal reset. For this, we change the gate-voltage from $V_G = 3$ V to $V_G = -5$ V and increase the source-drain voltage from $V_{SD} = 1$ V to $V_{SD} = 4$ V (red trace in Figure 2c). The fast initial drop in the red trace shows that the conductance decreases within tens of seconds to a steady-state value. This steady-state value corresponds to the initial conductance value as can be seen at the end of the red trace where the biasing was switched back to the sensing condition (transition from red trace to blue trace). Due to the small heat capacitance of CNTs,[24,25] current-induced heating leads to a rapid increase in the temperature of the CNTFET and the MOF/CNTFET interface. Cooling is also rapid since the heated active region is small and thermalized by the substrate and the metal electrodes. The dissipated electric power during sensing is only 1 pW in the off state and 20 nW in the on state, reaching 10 µW during resetting. The MOF/CNTFET are thus ultra-low power devices and dissipate orders of magnitude less power than MOF/GFETs.[2] We note that the reset cannot be accelerated merely by increasing the source-drain voltage since the current is required to stay high during the reset period. At $V_G = +3$ V, the current—and hence the power—would drop by orders of magnitude and the reset will not complete. Instead at $V_G = -5$V, the current and power reduce only moderately with time when resetting the device (transition from the orange to the blue curve in Figure 2a). The transconductance data of the reset device is shown in Figure S8, Supporting Information. Now, we address the sensitivity of the MOF/CNTFET to detect ethanol. Figure 2d shows the relative change in conductance $\Delta G/G$ when switching from $N_2$ to ethanol@$N_2$. $\Delta G/G$ is cal-

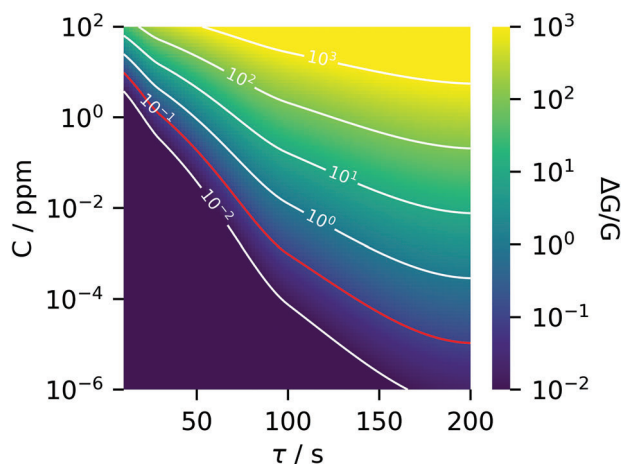**Table 1.** Parameters a and b to fit $\log(\Delta G/G) = a + b*\log(C)$ to the $\tau$-dependent data in Figure 2d.

| $\tau$ | a | b |
|---|---|---|
| 10 s | $3.19 \pm 0.02$ | $2.45 \pm 0.05$ |
| 30 s | $3.81 \pm 0.2$ | $1.82 \pm 0.47$ |
| 100 s | $4.14 \pm 0.02$ | $0.90 \pm 0.05$ |
| 200 s | $4.37 \pm 0.01$ | $0.70 \pm 0.025$ |

culated as $(G(C,\tau)-G(C=0))/G(C=0)$, where $C$ is the ethanol concentration and $\tau$ is the waiting time before taking the sensor reading, after switching to ethanol. We note that $C = 0.25$mg $L^{-1}$ ($\approx$100 ppm) is the lowest concentration reliably measurable with the commercial alcohol sensor that was used for gauging the MOF/CNTFET sensor. The double-logarithmic plot shows, that the relative change in conductance follows a power law with the exponent depending on the waiting time, $\tau$. The data fits to $\log(\Delta G/G) = a + b*\log(C)$ with the fit parameters $a$ and $b$ given in **Table 1**. From the inverse function $C = 10^{(\log(\Delta G/G) - a)/b}$, we calculate the detected concentration for specific values of $\tau$ and $\Delta G/G$. The values are given in **Table 2** and show a calculated device sensitivity of about 1 ppm for $\tau = 30$ s and $\Delta G/G = 10\%$, and below 1 ppt at $\tau = 200$ s and $\Delta G/G = 1\%$. Since our calibration curve is non-linear we approach the limit of detection (LOD) from the peak to peak noise of the baseline.[26,27] We have statistically analyzed the off-state conductance and find that $3\sigma$ is on the order of 10%, which corresponds to the middle row of Table 2. The LOD of a sensor is usually determined for steady-state conditions, hence we use $\tau = 200$ s data and find LOD $\approx$10 ppt. For other values of $\tau$ we refer to **Figure 3**, where we have calculated the sensor performance for the entire parameter space. The MOF/CNTFETs are ultra-sensitive devices due to the CNTFET's large on/off ratio and high sensitivity to charges, outperforming the MOF/GFETs by many orders of magnitude.[2] The sensor is also competitive to other types of ethanol sensors as shown in the comparison **Table 3**. Sensors based on pristine CNTFETs show only a weak response to ethanol,[28–31] and therefore only CNT-based sensors are listed where their response was enhanced by decoration with other materials or defect formation. Also not listed are MOF ethanol sensors that are based on capacitive and optical readout,[32,33] since those sensors appeared to be slow compared to an electrical readout of FET-type devices. Finally, we discuss the device performance under ambient conditions. The ultra-high sensitivity of a GFET to charges makes also this device susceptible to environmental changes when exposed to humidity and air, although the MOF

**Table 2.** Concentration of gaseous ethanol as calculated from $C = 10^{(\log(\Delta G/G) - a)/b} \cdot (100\text{ppm}/0.2\text{mg } L^{-1})$. $\Delta G/G$ is the relative change in conductance and $\tau$ is the waiting time before taking the sensor reading. The parameters a and b are taken as mean values from Table 1.

| $\Delta G/G$ | $\tau = 10$ s | $\tau = 30$ s | $\tau = 100$ s | $\tau = 200$ s |
|---|---|---|---|---|
| 100% | 24.9 ppm | 4.03 ppm | 12.6 ppb | 0.29 ppb |
| 10% | 9.75 ppm | 1.14 ppm | 0.97 ppb | 11 ppt |
| 1% | 3.81 ppm | 0.32 ppm | 75 ppt | 0.4 ppt |

**ADVANCED
SCIENCE NEWS**

www.advancedsciencenews.com

**ADVANCED
ELECTRONIC
MATERIALS**
Open Access

www.advelectronicmat.de

**Figure 3.** Limit of detection. The relative change in conductance $\Delta G/G$ is calculated for the concentration C and the waiting time $\tau$ before taking the sensor reading (details in Experimental Section). The red line denotes the limit of detection as derived from the peak to peak noise of the blank measurement baseline.

already greatly reduces this.[2] **Figure 4**a shows the shift in the threshold voltage and the increase of the hysteresis when changing from $N_2$ to ambient air. Nevertheless, the off-state remains accessible at $V_G > 4$ V. At the same time we observe, that the sensitivity to ethanol is not compromised by the humid air, since the four orders of magnitude change in the conductance is preserved. This is indicated in Figure 4b by the dashed arrow at the optimum gate voltage for sensing of $V_G \approx 5$ V. Hence the sensor is also operating under ambient conditions without loss of sensitivity. Let us finally revisit the surface chemistry that occurs on top of the CNTFET at the $Al_2O_3$/MOF interface, which is identical to the graphene-FET/$Al_2O_3$/MOF devices and which we have discussed previously in detail.[2] The chemisorption of alcohol on alumina causes the alcohol to split into $H^+$ and negatively charged alkoxy groups (alkoxy$^-$ such as ethoxy $C_2H_5O^-$). The negatively charged alkoxy$^-$ groups, which are weakly bound

to the alumina surface, diffuse away from the surface, as was observed in other experiments.[34] Hence during the exposure of the CNTFET with alcohol gas, the positive net charge is caused by the remaining $H^+$ at the alumina surface. Full coverage of a flat alumina surface due to chemisorption of alcohol would correspond to one pair of alkoxy$^-$ and $H^+$ adsorption sites per 26.4 $Å^2$, corresponding to $\approx 4 \times 10^{14}$ cm$^{-2}$ adsorption sites. Hence nominally less than 1% of the possible adsorption sites on alumina are required to be occupied with $H^+$ to induce the above-discussed channel charge accumulation, a number that is accessible at the $Al_2O_3$/MOF interface. In reality, there will be a concentration-dependent dynamic equilibrium since $H^+$ can be thermally desorbed and which is likely at the heart of the reset procedure. We do not know the charge distribution in the MOF but the MOF itself is not catalytically active and hence the charge accumulation has to be bound to the $Al_2O_3$/MOF interface. The conductivity in the CNT channel is therefore determined by the interplay between the charge accumulation at the $Al_2O_3$/MOF interface and the back-gate voltage. One can draw an analogy to a back-and-top-gated device and consider gate efficiencies and capacitances. For the 300 nm $SiO_2$ back-gate dielectric ($\varepsilon_r = 3.9\varepsilon_0$), the capacitance is 11.5 nF cm$^{-2}$. For the top 5 nm $Al_2O_3$ ($\varepsilon_r = 7.5\varepsilon_0$) one obtains 1326 nF cm$^{-2}$, and a capacitance ratio of 115. This means that to reach charge neutrality in a channel that has a positive charge accumulation on the order of $10^{12}$ cm$^{-2}$ it would require either a back-gate voltage of +15 V or a surface potential of +0.17 V at the $Al_2O_3$/MOF interface. For deeper insights into the chemical processes, we performed molecular dynamics simulations of the interaction of alcohol molecules with the crystalline MOF material.[2] The results were however not enlightening since the critical part of the sensor is the $Al_2O_3$/MOF interface, which is highly disordered because of the amorphous nature of the ALD-grown $Al_2O_3$ layer. As of now, we do not know the precise molecular structure which would be required for a simulation. However, we can nevertheless consider in more detail the dynamics of the device. The sensor responds to charge accumulation and hence to the charging of adsorption sites at the $Al_2O_3$/MOF interface, which in turn depends on the diffusion of ethanol molecules through the

**Table 3.** Comparison of ethanol sensors.

| Material | Response time | Operating temperature | Level of detection | Reference |
|---|---|---|---|---|
| Ag/In$_2$O$_3$ | 8 s@50 ppm | 220° | 50 ppm | [38] |
| MoS$_2$/ZnO | 30 s@500 ppm | 220° | 500 ppm | [39] |
| Fe$_2$O$_3$/SnO$_2$ | 9 s@100 ppm | 320° | 2 ppm | [40] |
| ZnO/SnO$_2$ | 1 s@30 ppm | 225° | 0.5 ppm | [41] |
| Pt-Pd/MWCNTs | Not specified | 25° | 3 ppm | [42] |
| ZnO/MWCNTs | 4 s@300 ppm | 260° | 1 ppm | [43] |
| SnO$_2$/MWCNTs | 150 s@not specified | 350° | not specified | [44] |
| Defective MWCNTs | 92 s@50 ppm | 30° | 5 ppm | [30] |
| Defective SWCNTs | 60 s@500 ppm | 22° | Not specified | [31] |
| Carbon nanobuds | 60 s@50 ppm | 22° | 50 ppm | [31] |
| GrO/aniline | 0.03 s@500 ppm | 25° | 500 ppm | [45] |
| Gr/ZnO NWs | Not specified | 125° | 1 ppm | [46] |
| MOF/graphene | 5 s@100 ppm | 25° | 100 ppm | [2] |
| MOF/CNT | 10 s@10 ppm | 25° | $\ll$1 ppb | this work |
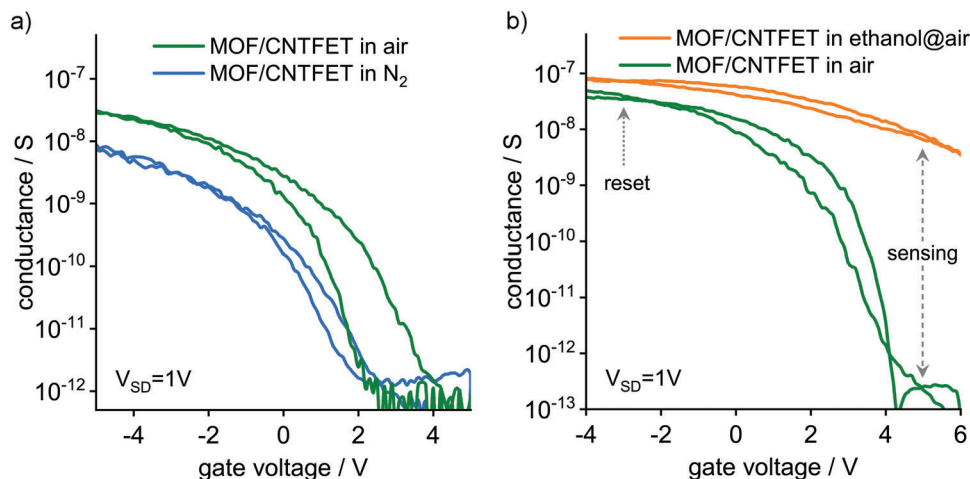
**Figure 4.** Response in ambient environment. a) transconductance measured in $N_2$ and in ambient air, b) transconductance measured in ethanol in ambient air and in ambient air ($\approx$30% humidity). Optimum gate voltages for sensing and reset are indicated.

MOF layer. At the $Al_2O_3$/MOF interface, the ethanol molecules are then catalytically split into $H^+$ and alkoxy$^-$, which eventually leads to a charging of the adsorption sites as discussed above. Such a problem can be described as a homogeneous diffusion problem,[35,36] and written as $\partial C/\partial t = D\nabla^2 C - \partial N/\partial t$, where $D$ is the diffusion coefficient, and $C$ the concentration of ethanol molecules that are free to move in the MOF layer. $N$ is the concentration of the ethanol molecules immobilized at the adsorption sites at the $Al_2O_3$/MOF interface, which after reaction form charged sites. The full solution of the problem has to include the reaction kinetics and is non-trivial, however, one can consider the diffusion-rate limited case and the reaction-rate limited case. When the diffusion is slow and the reaction kinetics reach rapid equilibrium ($\partial N/\partial t = 0$), then the formation of charged adsorption sites follows the ethanol concentration in the MOF layer and can be described by the Freundlich adsorption isotherm as $N = N_0 K C^X$, where $N_0$ is the total number density of adsorption sites, $X$ is the power index, and $K$ is the adsorption coefficient.[36] In this case, the process of charge accumulation simply slows down to the diffusion process in a plane sheet,[35] and the response time then depends on the thickness of the MOF layer, the diffusion constant, and importantly on the ethanol concentration $C_0$ above the MOF layer in the gas stream. In our experiment, we observe that the response time indeed depends strongly on the ethanol concentration $C_0$ and we therefore consider that our sensor operates in the diffusion-limited case. In the rate-limited case, the response time would not depend on the concentration and follow the Elovich equation.[36] This discussion explains that for a sensor operating in the diffusion limit, a longer waiting time is inevitably required for measuring lower concentrations. There are nevertheless options to reduce the waiting time. One way is to reduce the thickness of the MOF layer. We anticipate that a 10 nm thin MOF layer is sufficiently thick to preserve the sensor performance in terms of sensitivity against ethanol and insensitivity against moisture, and at the same time would reduce the response time by one order of magnitude. In addition, or alternatively, one can reduce the measurement time by using transient analysis in combination with a so-called Cantor pairing function, as has been introduced recently.[37]

## 3. Summary

The functionalization of semiconducting carbon nanotube transistors with metal–organic frameworks enabled the realization of a MOF-based ethanol sensor with outstanding properties, outperforming graphene-based MOF/GFETs by several orders of magnitude with respect to sensitivity and power consumption. Depending on the waiting time before taking the sensor reading, the detection of extremely low ethanol concentrations down to sub-ppb levels is possible. The exceptional sensor performance results from the nanotube transistor's high on/off ratio and its high sensitivity to charges. Remarkably, the MOF/CNTFET sensor works equally well in humid air, because the ambient-induced shift in threshold voltage was compensated without deteriorating the ethanol-induced change in conductance. Also remarkable is the exceptionally low power consumption, ranging between picowatt and nanowatt during sensing and microwatt during the current-induced resetting. We expect that with this novel concept of MOF/CNTFETs a variety of ultra-sensitive and ultra-low power sensors can be created by customizing MOF/CNTFET for specific gaseous analytes.

## 4. Experimental Section

*Device Fabrication*: MOF/CNTFET devices were fabricated on 300 nm thermal $SiO_2$ / 381 µm <100 > Si (p/B-doped, 0.005 Ω cm, Active Business Company) using electron-beam lithography (EBL). For all EBL steps, resist layers of poly(methyl methacrylate) (PMMA) 950k (Allresist) diluted in anisole were spin-casted, and pre-baked on a hot plate for 3 min at 150 °C. The e-beam exposed areas were developed in a solution of methyl isobutyl ketone/isopropanol (MIBK/IPA) at 0 °C for 30 s, rinsed with IPA, and dried in a nitrogen stream giving the required patterned structure. In the first step, the source–drain electrodes with 1 µm gap size, alignment markers, and the back gate contacts were defined. A scratch through the $SiO_2$ was made to contact the p-Si as a global back-gate from the top. After

**ADVANCED**
**SCIENCE NEWS**

www.advancedsciencenews.com

**ADVANCED**
**ELECTRONIC**
**MATERIALS**

www.advelectronicmat.de

spin-coating PMMA A4.5 at 6000 rpm for 60 s, e-beam exposure, and development, 3 nm Cr and 42 nm Pd were deposited by sputtering (Bestec; 100 W, RF, 30 s, and 70 W, DC, 45 s, respectively). Then, SWCNTs were site-selectively placed from suspension in between source–drain electrodes by using electric field-assisted dielectrophoresis (DEP).[16] The SWCNT suspension (preparation described below) was diluted prior to deposition by a factor of 100–200. Fifteen μL of suspension was drop cast onto the device and a 50 Hz AC signal of $10V_{pp}$ was applied on the common drain and the back-gate electrodes by using Agilent 33250 function generator for 3 min. The samples were rinsed several times with toluene to remove polymer residue, dried in a nitrogen stream, and annealed at 150 °C for 15 min to improve the contact between SWCNT and Pd. A 5 nm aluminum oxide layer was grown with an atomic layer deposition system (Picosun R200 Advanced) by exposure to six cycles of trimethylaluminium (TMA) and ozone at 25 °C, followed by 75 cycles of TMA and $H_2O$ at 150 °C (pulse-time TMA, oxygen, water: 0.1 s, flow-rate TMA, oxygen: 100 sccm, flow-rate $H_2O$: 200 sccm, purge time: 6 s, power ozone generator =70%). Finally, the $Cu_2(BDC)_2$-MOF was grown on the CNTFET as described below.

*SWCNT Suspension*: The polymer-wrapped CNT suspension was prepared by shear force mixing of 52 mg of TUBALL (OCSiAl Europe, lot no. 109-16092015) with 40 mg poly[(9,9-dioctylfluorenyl-2,7diyl)-alt-co-(6,6′-(2-20-bipyridine))] (PFO-BPy, American Dye Source, lot no. 19L014A1) in 110 mL toluene for 62 h. Subsequently, the suspension was centrifuged in an SW-40-Ti rotor (Beckman-Coulter. Optima L-80 XP) at 45 500 g for 30 min at 20 °C. The supernatant was concentrated by filtration (nylon membrane, 0.2mm pore size), rinsed with toluene, and re-dispersed to reduce the excess polymer content. The absorbance spectrum was measured with a Cary 500 spectrometer using a quartz cuvette with a 1 cm path length.

*MOF Synthesis*: The MOF layer was grown by the layer-by-layer (LbL) synthesis as described by Liu et al.[18] First, the surface of the CNTFET devices was activated in a UV ozone cleaner (Ossila, Sheffield, UK) for 1 min to maximize the number of functional OH groups at the $Al_2O_3$ surface. Afterward, the devices were put immediately into a $1 \times 10^{-3}$ m of copper(ii) acetate $(Cu_2(OAc)_4(H_2O)_2)$ ethanol solution before the synthesis. Then, the devices were placed on the sample holder and subsequently sprayed with $1 \times 10^{-3}$ м $Cu(OAc)_2$ ethanolic solution for 15 s and with a $0.2 \times 10^{-3}$ м 1,4-benzene dicarboxylic acid (BDC) ethanol solution for 25 s at room temperature. The sample was thoroughly rinsed with pure ethanol between both steps to remove undercoordinated metal-nodes or organic linker molecules. This procedure was repeated (in total) 35 times to grow a nominally 100 nm thick layer.

*Structural Characterization*: Scanning electron microscopy (SEM) images were taken with a Zeiss Ultra plus SEM at 10 keV beam energy, at 45° tilt angle, and in-lens detection. Energy-dispersive X-ray (EDX) spectra were recorded with a Zeiss LEO 1530 SEM and an Oxford instruments X-maxN detector at 2.5 keV beam energy, and analyzed with AZtec software from Oxford instruments. Raman measurements were done under ambient conditions with a Renishaw inVia Raman microscope at 532 nm excitation wavelength, 3 mW power, 60 s integration time, and 20× magnification. X-ray diffraction (XRD) measurements were carried out in an out-of-plane geometry using a Bruker D8-Advance diffractometer equipped with a position-sensitive LynxEye detector in $\theta$–$2\theta$ geometry. A Cu-anode with a wavelength of $\lambda = 0.154$ nm was used. The samples were investigated with an angle increment of 0.02° and a scan speed of 4 s per step.

*Electrical Transport and Sensing Measurements*: The CNTFETs and MOF/CNTFETs were mounted to a ceramic chip carrier, wire bonded, and with the package mounted to a cavity of volume $\approx 1$ cm³. The cavity had an inlet and outlet as part of a gas line system as described by Ganzhorn et al.[19] A four-way valve enabled instantaneous switching between gases, and the conditions were controlled by pressure gauges and flow meters (dosing valves). All measurements were carried out at flow rates of 0.5 L min⁻¹ and a static gas pressure of 0.25 bar above atmospheric pressure. The dynamic pressure $(< 10^{-4}$bar$)$ was negligible. The gas in the cavity was exchanged within 0.1 s, setting the time resolution of the measurements. In the downstream, a humidity sensor (Bosch BMP280) and an alcohol sensor (NCD MQ-3) were mounted in an additional cav-

ity and monitored with a Raspberry Pi. For exposure to alcohol and water molecules, the liquids were filled into a bubbler and flown through with dry nitrogen. The concentration of molecules in the carrier gas was adjusted by the nitrogen flow rate and monitored by commercial sensors in the downstream. If not stated otherwise, the initial starting condition was flowing dry nitrogen, and measurements were taken ≈15 min after changes of conditions. Electrical transport measurements were carried out with an Agilent 4155C semiconductor parameter analyzer with TRIAX cabling, and back gate sweeps were conducted at source–drain voltages of 1 V. Time-dependent measurements were done at 1 s time intervals. All experiments were carried out at room temperature.

*Calculating the Limit of Detection*: Figure 3 is calculated by fitting interpolation functions to the $\tau$-dependent parameters $a$ and $b$ of Table 1. These functions are then used to calculate $\Delta G/G$ versus $C$ and $\tau$ using the code provided at https://github.com/krupke-group/MOF_CNTFET_LOD.

## Supporting Information

Supporting Information is available from the Wiley Online Library or from the author.

## Conflict of Interest

The authors declare no conflict of interest.

## Author Contributions

The experiments were conceived and designed by R.K. and S.K. Devices were fabricated and characterized by S.K. and S.D. The MOF synthesis was performed by A.C. with input from L.H. The CNT dispersion was prepared by L.W. with input from B.F. The manuscript was written by R.K. and S.K. with input from all co-authors.

## Data Availability Statement

The data that support the findings of this study are available from the corresponding author upon reasonable request.

[1] A. Paghi, S. Mariani, G. Barillaro, *Small* **2023**, *19*, 2206100.

[2] S. Kumar, Y. Pramudya, K. Müller, A. Chandresh, S. Dehm, S. Heidrich, A. Fediai, D. Parmar, D. Perera, M. Rommel, L. Heinke, W. Wenzel, C. Wöll, R. Krupke, *Adv. Mater.* **2021**, *33*, 2103316.

[3] F. Schedin, A. K. Geim, S. V. Morozov, E. W. Hill, P. Blake, M. I. Katsnelson, K. S. Novoselov, *Nat. Mater.* **2007**, *6*, 652.

[4] J.-R. Li, R. J. Kuppler, H.-C. Zhou, *Chem. Soc. Rev.* **2009**, *38*, 1477.

[5] F. Hennrich, W. Li, R. Fischer, S. Lebedkin, R. Krupke, M. M. Kappes, *ACS Nano* **2016**, *10*, 1888.

[6] G. J. Brady, A. J. Way, N. S. Safron, H. T. Evensen, P. Gopalan, M. S. Arnold, *Sci. Adv.* **2016**, *2*, e1601240.

[7] S. Heinze, J. Tersoff, R. Martel, V. Derycke, J. Appenzeller, P. Avouris, *Phys. Rev. Lett.* **2002**, *89*, 106801.

[8] D. D. Chronopoulos, H. Saini, I. Tantis, R. Zbořil, K. Jayaramulu, M. Otyepka, *Small* **2022**, *18*, 2104628.

[9] H. Yuan, N. Li, W. Fan, H. Cai, D. Zhao, *Adv. Sci.* **2022**, *9*, 2104374.

[10] G. Wu, J. Huang, Y. Zang, J. He, G. Xu, *J. Am. Chem. Soc.* **2017**, *139*, 1360.

[11] G. A. Bodkhe, M. A. Deshmukh, H. K. Patil, S. M. Shirsat, V. Srihari, K. K. Pandey, G. Panchal, D. M. Phase, A. Mulchandani, M. D. Shirsat, *J. Phys. D: Appl. Phys.* **2019**, *52*, 335105.

[12] B. Wang, Y. Luo, B. Liu, G. Duan, *ACS Appl. Mater. Interfaces* **2019**, *11*, 35935.

[13] J. Mu, X. Zhong, W. Dai, X. Pei, J. Sun, J. Zhang, W. Luo, W. Zhou, *Molecules* **2022**, *27*, 2131.

[14] Z.-G. Gu, S.-C. Chen, W.-Q. Fu, Q. Zheng, J. Zhang, *ACS Appl. Mater. Interfaces* **2017**, *9*, 7259.

[15] B. Wang, H. Li, H. Tan, Y. Gu, L. Chen, L. Ji, Z. Sun, Q. Sun, S. Ding, D. W. Zhang, H. Zhu, *ACS Appl. Mater. Interfaces* **2022**, *14*, 42356.

[16] W. Li, F. Hennrich, B. S. Flavel, S. Dehm, M. Kappes, R. Krupke, *Nano Res.* **2021**, *14*, 2188.

[17] O. Shekhah, H. Wang, D. Zacher, R. A. Fischer, C. Wöll, *Angew. Chem., Int. Ed.* **2009**, *48*, 5038.

[18] J. Liu, B. Lukose, O. Shekhah, H. K. Arslan, P. Weidler, H. Gliemann, S. Bräse, S. Grosjean, A. Godt, X. Feng, K. Müllen, I.-B. Magdau, T. Heine, C. Wöll, *Sci. Rep.* **2012**, *2*, 921.

[19] M. Ganzhorn, A. Vijayaraghavan, S. Dehm, F. Hennrich, A. A. Green, M. Fichtner, A. Voigt, M. Rapp, H. von Löhneysen, M. C. Hersam, M. M. Kappes, R. Krupke, *ACS Nano* **2011**, *5*, 1670.

[20] J. E. Mondloch, O. Karagiaridi, O. K. Farha, J. T. Hupp, *CrystEngComm* **2013**, *15*, 9258.

[21] L.-l. Chua, J. Zaumseil, J.-f. Chang, E. C.-W. Ou, P. K.-H. Ho, H. Sirringhaus, R. H. Friend, *Nature* **2005**, *434*, 194.

[22] W. Kim, A. Javey, O. Vermesh, Q. Wang, Y. Li, H. Dai, *Nano Lett.* **2003**, *3*, 193.

[23] S. H. Jin, A. E. Islam, T.-i. Kim, J.-h. Kim, M. A. Alam, J. A. Rogers, *Adv. Funct. Mater.* **2012**, *22*, 2276.

[24] S. Zhang, M. Xia, S. Zhao, T. Xu, E. Zhang, *Phys. Rev. B* **2003**, *68*, 075415.

[25] F. Pyatkov, S. Khasminskaya, V. Kovalyuk, F. Hennrich, M. M. Kappes, G. N. Goltsman, W. H. P. Pernice, R. Krupke, *Beilstein J. Nanotechnol.* **2017**, *8*, 38.

[26] D. MacDougall, W. B. Crummett, Joginder Lal, Francis J. Amore, Donald G. Crosby, Francis L. Estes, David H. Freeman, William E. Gibbs, Glen E. Gordon, Lawrence H. Keith, Ralph R. Langner, Nina I. McClelland, Wendell F. Phillips, Robert B. Pojasek, Robert E. Sievers, Robert G. Smerko, David C. Wimert, Herbert A. Laitinen, Michael M. Reddy, Robert Libby, John K. Taylor, *Anal. Chem.* **1980**, *52*, 2242.

[27] G. L. Long, J. D. Winefordner, *Anal. Chem.* **1983**, *55*, 712A.

[28] T. Someya, J. Small, P. Kim, C. Nuckolls, J. T. Yardley, *Nano Lett.* **2003**, *3*, 877.

[29] S. J. Young, Z. D. Lin, *Microsyst. Technol.* **2018**, *24*, 55.

[30] N. M. Shaalan, F. Ahmed, O. Saber, S. Kumar, A. Aljaafari, A. Ashoaibi, A. Z. Mahmoud, M. Ezzeldien, *Materials* **2022**, *15*, 4439.

[31] I. V. Anoshkin, A. G. Nasibulin, P. R. Mudimela, M. He, V. Ermolov, E. I. Kauppinen, *Nano Res.* **2013**, *6*, 77.

[32] M. Hosseini, S. Zeinali, M. Sheikhi, *Sens. Actuators, B* **2016**, *230*, 9.

[33] G. Lu, J. T. Hupp, *J. Am. Chem. Soc.* **2010**, *132*, 7832.

[34] J. Van Tassel, C. Randall, *J. Colloid Interface Sci.* **2001**, *241*, 302.

[35] J. Crank, *The Mathematics of Diffusion*, Oxford University Press, Cary, NC **1986**.

[36] J. W. Gardner, M. Z. Iskandarani, B. Bott, *Sens. Actuators, B* **1992**, *9*, 133.

[37] S. Kanaparthi, S. G. Singh, *ACS Meas. Sci. Au* **2022**, *2*, 113.

[38] X. Liu, X. Sun, X. Duan, C. Zhang, K. Zhao, X. Xu, *Sens. Actuators, B* **2020**, *305*, 127450.

[39] Z. Song, J. Zhang, J. Jiang, *Ceram. Int.* **2020**, *46*, 6634.

[40] X. Liu, J. Zhang, X. Guo, S. Wang, S. Wu, *RSC Adv.* **2012**, *2*, 1650.

[41] J. Liu, T. Wang, B. Wang, P. Sun, Q. Yang, X. Liang, H. Song, G. Lu, *Sens. Actuators, B* **2017**, *245*, 551.

[42] Q. Nie, W. Zhang, L. Wang, Z. Guo, C. Li, J. Yao, M. Li, D. Wu, L. Zhou, *Sens. Actuators, B* **2018**, *270*, 140.

[43] H. Shan, C. Liu, L. Liu, L. Wang, X. Zhang, X. Chi, X. Bo, K. Wang, *Chin. Sci. Bull.* **2014**, *59*, 374.

[44] S. Ahmadnia-Feyzabad, A. A. Khodadadi, M. Vesali-Naseh, Y. Mortazavi, *Sens. Actuators, B* **2012**, *166–167*, 150.

[45] X. Zhu, J. Zhang, Q. Xie, Z.-L. Hou, *ACS Appl. Mater. Interfaces* **2020**, *12*, 38708.

[46] Z. Rafiee, H. Roshan, M. H. Sheikhi, *Ceram. Int.* **2021**, *47*, 5311.